

Neutron-quark stars: Discerning viable alternatives for the higher-density part of the equation of state of compact stars

Sudipta Hensh,^{1,2,*} Yong-Jia Huang,^{3,4,†} Toru Kojo,^{5,‡} Luca Baiotti,⁶
Kentaro Takami,^{7,4} Shigehiro Nagataki,^{2,4,8} and Hajime Sotani^{2,4}

¹*Department of Earth and Space Science, Graduate School of Science,
Osaka University, 1-1 Machikaneyama-cho, Toyonaka, Osaka 560-0043, Japan*

²*Astrophysical Big Bang Laboratory (ABBL), RIKEN Cluster for Pioneering Research, 2-1 Hirosawa, Wako, Saitama 351-0198, Japan*

³*Key Laboratory of Dark Matter and Space Astronomy,*

Purple Mountain Observatory, Chinese Academy of Science, Nanjing, 210008, China

⁴*RIKEN Interdisciplinary Theoretical and Mathematical Sciences Program (iTHEMS), RIKEN, Wako 351-0198, Japan*

⁵*Department of Physics, Tohoku University, Sendai, 980-8578, Japan*

⁶*International College and Graduate School of Science, Osaka University,
1-2 Machikaneyama-cho, Toyonaka, Osaka 560-0043, Japan*

⁷*Kobe City College of Technology, 651-2194 Kobe, Japan*

⁸*Astrophysical Big Bang Group (ABBG), Okinawa Institute of Science and Technology (OIST),
1919-1 Tancha, Onna-son, Kunigami-gun, Okinawa 904-0495, Japan*

(Dated: August 5, 2024)

By taking into account the latest observations and theoretical constraints, we investigate the merger and post-merger of binary neutron stars (NSs) with general-relativistic numerical simulations employing hadronic and hybrid equations of state (EOSs). We name our hybrid stars *neutron-quark stars* (NQS), because the transition from hadrons to quarks starts at a density lower than the central density of $\sim 1M_{\odot}$ stars. We address two viable scenarios for the transition to quark matter: a crossover or a strong first-order phase transition (IPT). We find that a crossover transition is in principle observable when both the inspiral and post-merger signals are detected because the post-merger gravitational-wave (GW) main frequency f_2 is generally lower than that of hadronic models with the same tidal deformability (Λ). Since it is viable according to current multi-messenger constraints, we also highlight the possibility of an EOS with a strong IPT that takes place at 1.8 times the nuclear saturation density, with a stiff quark EOS after the transition. It is the first time that mergers of binary NQSs with a deconfined quark-matter core are studied numerically in full general relativity. In this case, although $(\Lambda, \text{compactness})$ lies significantly outside the hadronic relation, (Λ, f_2) is close to the relation valid for hadronic EOSs. We also point out a linear correlation, valid within the observational constraints and not sensitive to the presence of a hadron-quark transition, between the emitted energy in GWs and their frequency.

Introduction. Neutron stars (NSs), composed of cold, dense matter at a few times nuclear saturation density ($n_0 \simeq 0.16 \text{ fm}^{-3}$), are cosmic laboratories for exploring dense matter in quantum chromodynamics (QCD) [1, 2]. Recent dramatic progress in observations has significantly advanced our understanding of NS macroscopic properties, determining some of their characteristics with notable precision [3–10]. Combined with nuclear constraints at $\sim n_0$, the uncertainty in radius has been narrowed to approximately 1 km for NSs with masses in the range 1.4–2.0 M_{\odot} at 90% confidence level [11, 12]. These observations begin to allow discrimination between EOSs containing different microscopic degrees of freedom.

Joint information, including the NICER mass-radius inference of PSR J0030+0451, PSR J0740+6620 and PSR J0437-4715 [5–9], tidal deformability from the GW170817 event [4], and *ab-initio* calculations from nuclear physics, such as chiral effective field theory (ChEFT) [13] near n_0 and perturbative QCD (pQCD) at ultra-high densities [14, 15], have provided statistical constraints on the EOSs and the associated sound speed in a model-agnostic manner. The square of the speed of sound c_s^2 versus den-

sity around 2–4 n_0 has been found to be nonmonotonic, featuring at least one peak, exceeding the conformal limit ($c_s^2 = c^2/3$) [12, 16–19], suggesting that the matter within massive NSs is not purely hadronic. Indeed, the observationally preferred EOS stiffens at a rate greater than predicted by typical nucleonic descriptions. This result arises from statistical analyses taking into account the existence of a NS with 2.08 M_{\odot} [20] (or $\sim 2.3M_{\odot}$, from the optical lightcurve of the black widow pulsar [21], or mass function [22, 23]), the stringent theoretical and experimental constraints around n_0 , and the fact that the radii for a 1.4 and a 2.1 M_{\odot} NS are found to be similar [10, 12, 24]. The EOS softening in massive NSs, instead, stems from the pressure constraint from pQCD. Therefore, conventional first-order phase transitions (IPTs) occurring at an intermediate density, where the observed c_s^2 peak is located, are disfavored, as such transitions involve a jump in energy density and thus induce EOS softening instead. To reconcile rapid stiffening with the expected appearance of quark degrees of freedom, quark-hadron crossover (QHC) scenarios are proposed [25–27], which, unlike IPT models, stiffen the EOS during the hadron-quark transition [28, 29].

However, it is difficult to gain information on the high-density part of the stellar EOS only from observation of NSs in equilibrium, because a direct measurement of the maximum mass for a non-rotating NS is hard, and such measurement may not be sensitive to the state of matter at the NS center [30, 31]. Theoretical limits on the EOS depend somewhat on the implementation of pQCD constraints, which remain debated [32, 33]. Instead, we may obtain more accurate information of the hadron-quark transition from binary neutron star (BNS) mergers [34–44], whose post-merger GW spectrum exhibits several peaks [45–50], the frequency of the main of which, indicated often as f_2 , may be observed relatively cleanly, with the sensitivities expected to be reached in third-generation detectors, such as Einstein Telescope [51], Cosmic Explorer [52], or NEMO [53].

In this letter, we study mergers of binaries composed of inspiralling compact stars that contain quark degrees of freedom, namely *neutron-quark stars* (NQSs). The name is related to the fact that, transitions from hadrons to quarks starting at a density lower than that at the center of the lightest NSs would yield M - R curves that are similar to hadronic ones [10, 12, 24]. Quark degrees of freedom, whether or not they are completely deconfined, are likely always present in compact stars. This is evident also from the upper panel of Fig. 1, where open circles show stars whose central density is $2n_0$. All of them lie much below the lowest mass of known NSs. For the first time to the best of our knowledge, we present general-relativistic simulations of NQSs with a 1PT and NQSs with the QHC EOS of [27], in addition to NSs with purely nucleonic EOSs, for comparison.

To avoid model-dependent phenomena in finite temperature EOSs, we mimic thermal effects through an ideal-gas approximation with a fixed thermal index $\Gamma = 2$, as in our previous work [37] and as commonly done in the literature. In 1PT scenarios (as studied, *e.g.*, in [54, 55]), it is thought that finite-temperature effects lower the onset of the transition, potentially causing significantly higher f_2 than that of the baseline EOS¹. However, how much the onset density is affected by finite-temperature effects is beyond the reach of observations of NSs in equilibrium. In this work, by adopting a fixed onset density through an ideal-gas thermal treatment, the simulation results reflect the properties of cold EOSs, in particular, providing a conservative estimate for the difference in f_2 in NSs and NQSs. We expect that finite-temperature effects would yield larger post-merger frequency differences.

Equations of State and simulation setup. For the codes used and the numerical setup, see Sect. II in the supplemental material (SM).

¹ The *baseline* of an EOS containing quarks is the nucleonic EOS used for lower densities.

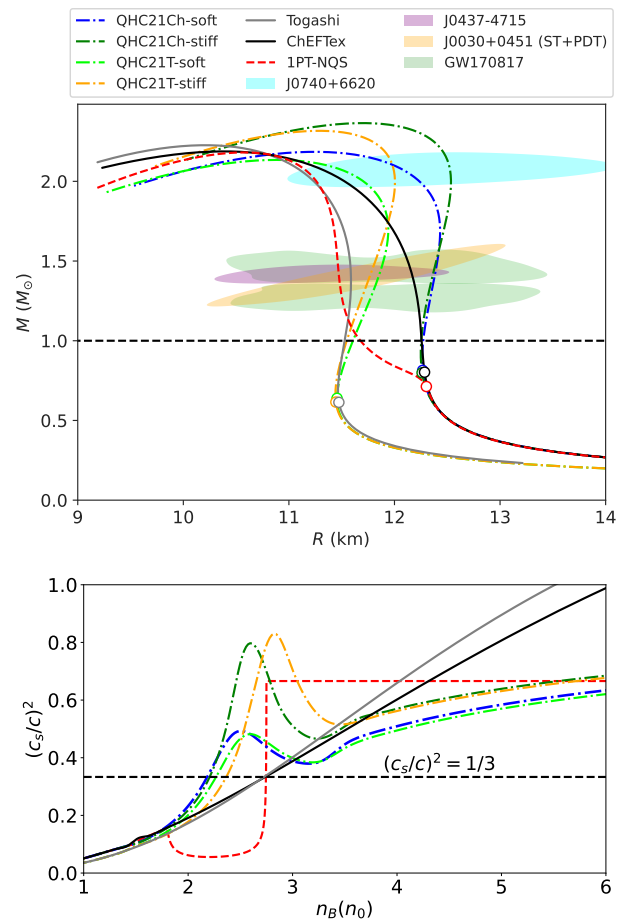


FIG. 1. *Upper panel:* The M - R relation for the NS and NQS models in this work, as well as the 68% confidence interval from some observations. Open circles represent the theoretical NSs whose central density is $2n_0$. *Lower panel:* The square of the sound speed as a function of baryon number density n_B for the various EOSs. The dashed line represents the conformal limit $(c_s/c)^2 = 1/3$ [56].

As highlighted in Fig. 1, all the EOS models used here satisfy current multi-messenger constraints, including the maximum mass for a non-rotating NS, and the tidal deformability and the radius for a $1.4M_\odot$ NS, according to the new NICER radius estimates for PSR J0437-4715 ($11.36^{+0.95}_{-0.63}$ km) [9] and PSR J0030+0451 ($11.71^{+0.88}_{-0.83}$ km in the ST+PDT model) [57], which are more consistent with the findings from the GW170817 event [4] and slightly smaller than previous estimates [6, 8]. The hadronic baseline EOSs for our NQS models are either the Togashi EOS [58] or an EOS based on the latest N3LO ChEFT results [59–61], which we name ChEFTex because we extended it to higher densities to be able to follow the merged object. Both of these are consistent with our current theoretical understanding of the EOS up to near n_0 . Note that EOSs that differ significantly in the $c_s^2(n_B)$ relation (bottom panel of Fig. 1) are rather similar in the observable region

of the M - R plane.

The details of how the EOSs were constructed can be found in the SM. Here, we briefly introduce the main features of our NQS models. In case a strong 1PT EOS occurs, the radius of a high-mass NS is usually remarkably smaller than that of a low-mass NS. In order for this to be compatible with current observations, such 1PT is likely to occur either at the highest densities near the center of massive NSs or in a lower-density region and with a stiff quark-matter EOS [12]. Since we are interested in post-merger GWs, we consider here only the latter scenario; the former leads inevitably to prompt collapse to a black hole. Therefore, in our 1PT model a quark matter core is already present during the inspiral. The phase transition starts at $\sim 1.8n_0$ and ends at $\sim 2.75n_0$, at densities higher than which a stiff quark EOS $c_s^2 = 2/3 c^2$ is adopted. We call this EOS the 1PT-NQS.

Another possible mechanism for the hadron-quark transition is a QHC, whose most remarkable feature is the rapid stiffening and the associated sound-speed peak occurring in the region between the nuclear- and quark-matter domains (see Fig 1). The rapid stiffening leads to the radius of a $2.0M_\odot$ NS being similar or even larger than that of a $1.4M_\odot$ NS.

We consider two of the QHC21 models obtained with different parameters in [27]: the A models and the D models, which are, respectively, the softest and the stiffest in the sound-speed peak region. For each of them, we consider models with both alternatives for the baseline EOS: the Togashi EOS and the ChEFTex EOS. For these four models, we use the names QHC21Ch-soft, QHC21Ch-stiff, QHC21T-soft, and QHC21T-stiff, respectively.

We study equal-mass BNS systems with three total masses: *low* ($2.5M_\odot$ for all models), *intermediate* ($2.75M_\odot$ for all models) and *high* (2.86 – $2.96M_\odot$). The choice of the masses in the high range was made so that for each EOS the collapse occurs late enough to accurately compute the post-merger frequency f_2 . This was possible only for the QHC models in that mass range.

Results and discussion. An overview of the matter evolution is presented in the SM, also with 2D figures.

We compute the spectrum of the fundamental and dominant harmonic mode ($l = m = 2$) of the GW strain up to 18 ms after the merger for all models except for QHC21Ch-soft with mass $2.96M_\odot$, where the collapse to black hole occurs around 11 ms after the merger.

The values of f_2 are estimated by fitting the spectrum through the Markov Chain Monte Carlo method described in the SM of [37], in which the GW contribution from the inspiral is filtered out by approximating it with a power law plus exponential decay (starting at the contact frequency), and the main peak is described by a skewed Gaussian. For a more direct comparison with other works, we also compute the mean of the f_2 frequency, $f_{2,\text{mean}}$, following the definition of Eq. (21) in [48].

Although the degrees of freedom in NSs and NQSs are

different, their mass-radius curves could be similar (see Fig. 1), but joint information from before and after the merger can help discriminate the EOS. In Fig. 2, we plot the tidal deformability (Λ) versus $f_{2,\text{mean}}$ for both hadronic and NQS EOSs. For the former, we show the results for the ChEFTex EOS, the Togashi EOS, and the three EOSs (SLy [62], APR4 [63], and LS220 [64]) studied in [50] that are still compatible with current observational constraints [12]. We consider the linear fitting $f_{2,\text{mean}} = \alpha + \beta \Lambda$, where α , and β are parameters determined by fitting only the hadronic models. The best fits with their standard error are $\alpha = 3678.43 \pm 83.97$ Hz and $\beta = -0.83 \pm 0.16$ Hz, respectively. Note that the residual of the fitting of hadronic models will become smaller with further multi-messenger observations of NSs, since some of these models will be excluded by improved determination of the M - R curve.

Inspecting the $f_{2,\text{mean}}$ - Λ relation, we notice that the QHC models show generally lower f_2 than the best-fit curve for hadronic models. The QHC models with the strongest stiffening lie outside the lower bound of the one-standard-deviation error region by more than 200 Hz. Note that the numerical uncertainty due to finite resolution in our simulations is estimated to be at most 50 Hz (this occurs for the M1375 QHC21Ch-soft model, with the highest resolution having a lower frequency).

The $f_{2,\text{mean}}$ for the 1PT-NQS models are about 300 Hz higher than their hadronic baseline (see Table I in the SM), but the 1PT-NQS models are still compatible with the best-fit curve for the hadronic models. This is mainly because the stiffness of the 1PT-NQS models is similar before and after the merger, since in both phases the stellar core is already in the density region where $c_s = 2/3 c^2$. We empha-

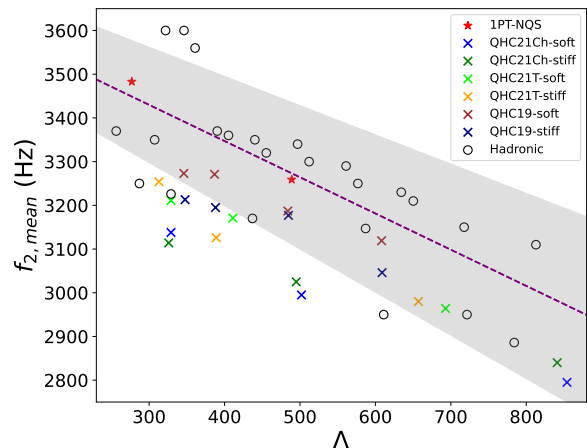


FIG. 2. Scatter plot of $f_{2,\text{mean}}$ and dimensionless tidal deformability. Hadronic EOSs include our Togashi and ChEFTex EOSs, and the SLy, APR4, and LS220 EOSs, from [50]. Data for the QHC19 models are from [37]. The dashed line shows the best-fit curve considering the hadronic models only. The shaded area shows the maximum residual of the fitting.

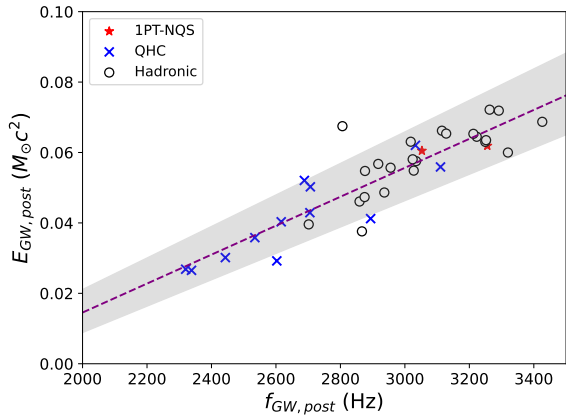


FIG. 3. Scatter plot of GW energy released in the post-merger $E_{GW,post}$ and instantaneous frequency $f_{GW,post}$. $E_{GW,post}$ is calculated as the difference between the energy emitted in GWs at the end of the simulation (when further emission is negligible, see Fig. S8 in the SM) and that emitted until the time of the merger, from the $l = m = 2$ mode (emission in other modes is negligible). $f_{GW,post}$ is the average GW frequency in the last 5 ms of the simulation. The dashed line shows the best-fit curve.

size again that ours is a conservative estimation, where a temperature-dependent phase boundary and more complex quark EOSs have not been considered.

Although the early presence of quark matter in the 1PT-NQS model may not be observable from the $\Lambda - f_2$ relation, the mass distribution for NQSs is undoubtedly different from that of NSs based on a nucleonic description. In Fig. S6 of the SM, we show the relation between Λ and the compactness of a star with gravitational mass equal to that of one of the stars in the binary when isolated. We note that the 1PT-NQS EOS is an outlier in this relation (while the QHC EOSs lie near the best-fit curve). This means that, for example, the inferred radius from a Λ measurement performed from GW detectors would be underestimated for the 1PT-NQS model. A measured Λ that corresponds to a radius (measured, *e.g.*, by NICER) larger than that expected from the Λ -compactness relation would be in support of the 1PT-NQS scenario.

Another quantity of interest is the energy emitted in post-merger GWs and its relation to the nature of hadron-quark transitions. Energy emission in post-merger GWs may be related to electromagnetic signals from binary NS/NQS mergers and the latter may provide useful information for studying the central engine of γ -ray bursts [65, 66]. Since it is hard to analytically describe the non-linear oscillations occurring after the merger, using our simulation results, we propose a method to estimate the energy emitted in GWs in the early post-merger phase, based only on a measurement of f_2 . In fact, in actual GW observations, only f_2 , and not the full waveform, may be measured with sufficient accuracy. GW energy is mainly released in the first ~ 10 ms after the merger (see also Fig. S8 in the SM).

Right after the merger, the GW frequency changes significantly because of the presence of multiple modes [49, 67], all of which are damped in a few ms, except for the f_2 mode. In Fig. 3, we show, for hadronic and NQS models, the scatter plot and the fitting of the energy released in GWs after the merger ($E_{GW,post}$) versus the instantaneous GW frequency ($f_{GW,post}$), averaged over the last 5 ms of the simulations (where, essentially, only the f_2 mode contributes). We used the same EOSs as in Fig. 2 for NS (with the addition of some non-equal-mass models from [50]) and NQS models. It is apparent that $E_{GW,post}$ is linearly correlated with $f_{GW,post}$ for all models with: $E_{GW,post} = 4.308 \times 10^{-5} (f_{GW,post} - 1687) (M_\odot c^2)$. The total GW energy emitted in the post-merger is $\sim 0.02 - 0.08 M_\odot c^2$. The 1PT-NQS/QHC EOSs are clustered around the high/low end in the frequency-energy plane, respectively. The relation is not sensitive to the presence of quark degrees of freedom, via 1PT or crossover, nor to the binary mass ratio.

Finally, we comment on the relation between the energy and the angular momentum radiated in GWs that was recently highlighted in [68] (see also [69, 70]). It is suggested that, at late times, different EOSs can be distinguished in such plots as they follow straight lines deviating from each other. In Fig. S9 of the SM, we show such a relation, also in a different form from [68], where quantities normalized to their values at the time of merger were displayed. Instead, we propose using the angular momentum and energy emitted after the merger (namely, subtracting the inspiral contribution) and without normalization, as shown in the lower panels of Fig. S9 of the SM. This is because the normalization procedure with respect to the value at the time of merger could be arbitrary. For example, if the same binary system is simulated for different numbers of orbits, the value of the angular momentum and energy radiated until merger would be different. In practice, we suggest to use the relation $E_{GW} - E_{GW}^{insp}$ vs. $J_{GW} - J_{GW}^{insp}$, where E_{GW}^{insp} (J_{GW}^{insp}) is the total energy (angular momentum) carried away by GWs in the inspiral phase.

Furthermore, we observe larger differences between our models when using non-normalized post-merger-only quantities (*cf.* Fig. S9 of the SM). In particular, with the relation we propose the curve for 1PT-NQS deviates considerably from the other models, especially in the intermediate-mass case.

Summary. In addition to some hadronic NS mergers, in this letter, we presented the first fully general-relativistic simulations of binary NQS mergers with EOSs compatible with current multi-messenger constraints and in which quark degrees of freedom are always present in isolated stars because of a 1PT or QHC [27]. We provided analyses that discriminate between many of the EOSs we studied. In particular, we showed that, in the $f_{2,mean} - \Lambda$ relation, QHC models stand out in general, and many of them lie significantly far from the best-fit curve for the hadronic models, suggesting that the presence of a QHC could be identified

if both inspiral and post-merger GW signals are detected.

On the other hand, the f_2 frequency for our 1PT-NQS model, despite being significantly higher than that of other models, is compatible with the $f_{2,mean} - \Lambda$ relation for hadronic EOSs. However, our 1PT-NQS model stands out from all other models in the Λ -compactness plot and thus could be identified by comparing tidal deformability measurements from BNS mergers and stellar-radius measurements from, *e.g.*, NICER.

In addition, we find a good linear correlation between instantaneous frequency and energy emitted in post-merger GWs. This could be used to estimate the emitted GW energy also in cases where only f_2 is measured accurately, rather than the whole post-merger strain. Finally, we propose a small modification to a recently proposed relation between the energy and angular momentum emitted in GWs. Our suggestion makes the relation less dependent on the initial conditions of the simulations and seems to highlight even further the differences due to EOSs.

Straightforward extensions to our work include studying the effects of varying the onset density of the 1PT and the binary mass ratio. Much more demanding, and interesting, would be extending the present analyses to NQS EOS at finite temperature.

ACKNOWLEDGMENTS

Our simulations were carried out on the Hokusai Big-waterfall supercomputer in RIKEN and the XC50 system at the Center for Computational Astrophysics (CfCA) of the National Astronomical Observatory of Japan (NAOJ). Y.H. would like to thank the stimulating discussions at the 2024 TDLI Workshop on Dense Matter Equation of State and Frontiers in Neutron Star Physics. S.H. is supported by the Japan Society for the Promotion of Science (JSPS) KAKENHI Grant No. 22F22750. Y.H. is supported by the National Natural Science Foundation of China No. 12233011 and by the Postdoctoral Fellowship Program of CPSF under Grant Number GZC20241915. T.K. is supported by the JSPS KAKENHI Grant No. 23K03377 and No. 18H05407 and by the Graduate Program on Physics for the Universe (GPPU) at Tohoku University. H.S. is supported by the JSPS KAKENHI Grant No. JP23K20848 and JP24KF0090, and by the FY2023 RIKEN Incentive Research Project. H.S. and S.N. are supported by the Pioneering Program of RIKEN for Evolution of Matter in the Universe (r-EMU). K.T. is supported by the JSPS KAKENHI Grant No. 17K14305 and 23K03399. K.T. and S.N. are supported by the JSPS KAKENHI Grant No. 19H00693.

* hensh@astro-osaka.jp, sudiptahensh2009@gmail.com

† huangyj@pmo.ac.cn

‡ toru.kojo.b1@tohoku.ac.jp

- [1] G. Baym, T. Hatsuda, T. Kojo, P. D. Powell, Y. Song, and T. Takatsuka, *Reports on Progress in Physics* **81**, 056902 (2018).
- [2] J. M. Lattimer, *Ann. Rev. Nucl. Part. Sci.* **71**, 433 (2021).
- [3] B. P. Abbott, R. Abbott, T. D. Abbott, and et al. (LIGO Scientific Collaboration and Virgo Collaboration), *Phys. Rev. Lett.* **119**, 161101 (2017).
- [4] B. P. Abbott *et al.* (LIGO Scientific, Virgo), *Phys. Rev. X* **9**, 011001 (2019), [arXiv:1805.11579 \[gr-qc\]](https://arxiv.org/abs/1805.11579).
- [5] T. E. Riley *et al.*, *Astrophys. J. Lett.* **887**, L21 (2019), [arXiv:1912.05702 \[astro-ph.HE\]](https://arxiv.org/abs/1912.05702).
- [6] M. C. Miller *et al.*, *Astrophys. J. Lett.* **887**, L24 (2019), [arXiv:1912.05705 \[astro-ph.HE\]](https://arxiv.org/abs/1912.05705).
- [7] T. E. Riley *et al.*, *Astrophys. J. Lett.* **918**, L27 (2021), [arXiv:2105.06980 \[astro-ph.HE\]](https://arxiv.org/abs/2105.06980).
- [8] M. C. Miller *et al.*, *Astrophys. J. Lett.* **918**, L28 (2021), [arXiv:2105.06979 \[astro-ph.HE\]](https://arxiv.org/abs/2105.06979).
- [9] D. Choudhury, T. Salmi, S. Vinciguerra, T. E. Riley, Y. Kini, A. L. Watts, B. Dorsman, S. Bogdanov, S. Guillot, P. S. Ray, D. J. Reardon, R. A. Remillard, A. V. Bilous, D. Huppenkothen, J. M. Lattimer, N. Rutherford, Z. Arzumanyan, K. C. Gendreau, S. M. Morsink, and W. C. G. Ho, *arXiv e-prints*, [arXiv:2407.06789](https://arxiv.org/abs/2407.06789) (2024), [arXiv:2407.06789 \[astro-ph.HE\]](https://arxiv.org/abs/2407.06789).
- [10] S.-P. Tang, Y.-J. Huang, M.-Z. Han, and Y.-Z. Fan, *arXiv e-prints*, [arXiv:2404.09563](https://arxiv.org/abs/2404.09563) (2024), [arXiv:2404.09563 \[astro-ph.HE\]](https://arxiv.org/abs/2404.09563).
- [11] I. Legred, K. Chatziioannou, R. Essick, S. Han, and P. Landry, *Phys. Rev. D* **104**, 063003 (2021), [arXiv:2106.05313 \[astro-ph.HE\]](https://arxiv.org/abs/2106.05313).
- [12] M.-Z. Han, Y.-J. Huang, S.-P. Tang, and Y.-Z. Fan, *Science Bulletin* **68**, 913 (2023), [arXiv:2207.13613 \[astro-ph.HE\]](https://arxiv.org/abs/2207.13613).
- [13] C. Drischler, K. Hebeler, and A. Schwenk, *Phys. Rev. Lett.* **122**, 042501 (2019).
- [14] A. Kurkela, P. Romatschke, and A. Vuorinen, *Phys. Rev. D* **81**, 105021 (2010).
- [15] T. Gorda, A. Kurkela, R. Paatelainen, S. Säppi, and A. Vuorinen, *Phys. Rev. Lett.* **127**, 162003 (2021), [arXiv:2103.05658 \[hep-ph\]](https://arxiv.org/abs/2103.05658).
- [16] S. Altiparmak, C. Ecker, and L. Rezzolla, *Astrophys. J. Lett.* **939**, L34 (2022), [arXiv:2203.14974 \[astro-ph.HE\]](https://arxiv.org/abs/2203.14974).
- [17] M. Omana Kuttan, J. Steinheimer, K. Zhou, and H. Stoecker, *Phys. Rev. Lett.* **131**, 202303 (2023), [arXiv:2211.11670 \[hep-ph\]](https://arxiv.org/abs/2211.11670).
- [18] L. Brandes, W. Weise, and N. Kaiser, *Phys. Rev. D* **108**, 094014 (2023), [arXiv:2306.06218 \[nucl-th\]](https://arxiv.org/abs/2306.06218).
- [19] E. Annala, T. Gorda, J. Hirvonen, O. Komoltsev, A. Kurkela, J. Nättilä, and A. Vuorinen, *Nature Commun.* **14**, 8451 (2023), [arXiv:2303.11356 \[astro-ph.HE\]](https://arxiv.org/abs/2303.11356).
- [20] H. T. Cromartie, E. Fonseca, S. M. Ransom, and et al., *Nature Astronomy* **4**, 72 (2020), [arXiv:1904.06759 \[astro-ph.HE\]](https://arxiv.org/abs/1904.06759).
- [21] R. W. Romani, D. Kandel, A. V. Filippenko, T. G. Brink, and W. Zheng, *Astrophys. J. Lett.* **934**, L17 (2022), [arXiv:2207.05124 \[astro-ph.HE\]](https://arxiv.org/abs/2207.05124).
- [22] D.-S. Shao, S.-P. Tang, J.-L. Jiang, and Y.-Z. Fan, *Phys. Rev. D* **102**, 063006 (2020), [arXiv:2009.04275 \[astro-ph.HE\]](https://arxiv.org/abs/2009.04275).
- [23] Y.-Z. Fan, M.-Z. Han, J.-L. Jiang, D.-S. Shao, and S.-P. Tang, *Phys. Rev. D* **109**, 043052 (2024).

- [24] N. Rutherford *et al.*, arXiv e-prints [10.48550/arXiv.2407.06790](https://arxiv.org/abs/10.48550/arXiv.2407.06790) (2024), [arXiv:2407.06790](https://arxiv.org/abs/2407.06790) [astro-ph.HE].
- [25] K. Masuda, T. Hatsuda, and T. Takatsuka, *PTEP* **2013**, 073D01 (2013), [arXiv:1212.6803](https://arxiv.org/abs/1212.6803) [nucl-th].
- [26] G. Baym, S. Furusawa, T. Hatsuda, T. Kojo, and H. Togashi, *Astrophys. J.* **885**, 42 (2019), [arXiv:1903.08963](https://arxiv.org/abs/1903.08963) [astro-ph.HE].
- [27] T. Kojo, G. Baym, and T. Hatsuda, *Astrophys. J.* **934**, 46 (2022), [arXiv:2111.11919](https://arxiv.org/abs/2111.11919) [astro-ph.HE].
- [28] T. Kojo, *Phys. Rev. D* **104**, 074005 (2021), [arXiv:2106.06687](https://arxiv.org/abs/2106.06687) [nucl-th].
- [29] Y. Fujimoto, T. Kojo, and L. D. McLerran, *Phys. Rev. Lett.* **132**, 112701 (2024).
- [30] M. Alford, M. Braby, M. W. Paris, and S. Reddy, *Astrophys. J.* **629**, 969 (2005), [arXiv:nucl-th/0411016](https://arxiv.org/abs/nucl-th/0411016).
- [31] J.-E. Christian, J. Schaffner-Bielich, and S. Rosswog, *Phys. Rev. D* **109**, 063035 (2024), [arXiv:2312.10148](https://arxiv.org/abs/2312.10148) [nucl-th].
- [32] R. Somasundaram, I. Tews, and J. Margueron, *Phys. Rev. C* **107**, 025801 (2023), [arXiv:2112.08157](https://arxiv.org/abs/2112.08157) [nucl-th].
- [33] O. Komoltsev, R. Somasundaram, T. Gorda, A. Kurkela, J. Margueron, and I. Tews, *Phys. Rev. D* **109**, 094030 (2024), [arXiv:2312.14127](https://arxiv.org/abs/2312.14127) [nucl-th].
- [34] A. Bauswein, N.-U. F. Bastian, D. B. Blaschke, K. Chatziioannou, J. A. Clark, T. Fischer, and M. Oertel, *Physical Review Letters* **122**, 061102 (2019).
- [35] L. R. Weih, M. Hanauske, and L. Rezzolla, *Phys. Rev. Lett.* **124**, 171103 (2020), [arXiv:1912.09340](https://arxiv.org/abs/1912.09340) [gr-qc].
- [36] E. R. Most, L. J. Papenfort, V. Dexheimer, M. Hanauske, S. Schramm, H. Stöcker, and L. Rezzolla, *Phys. Rev. Lett.* **122**, 061101 (2019), [arXiv:1807.03684](https://arxiv.org/abs/1807.03684) [astro-ph.HE].
- [37] Y.-J. Huang, L. Baiotti, T. Kojo, K. Takami, H. Sotani, H. Togashi, T. Hatsuda, S. Nagataki, and Y.-Z. Fan, *Phys. Rev. Lett.* **129**, 181101 (2022).
- [38] C. A. Raithel and E. R. Most, *Phys. Rev. Lett.* **130**, 201403 (2023), [arXiv:2208.04294](https://arxiv.org/abs/2208.04294) [astro-ph.HE].
- [39] Y. Fujimoto, K. Fukushima, K. Hotokezaka, and K. Kyutoku, *Phys. Rev. Lett.* **130**, 091404 (2023), [arXiv:2205.03882](https://arxiv.org/abs/2205.03882) [astro-ph.HE].
- [40] A. Kedia, H. I. Kim, I.-S. Suh, and G. J. Mathews, *Phys. Rev. D* **106**, 103027 (2022), [arXiv:2203.05461](https://arxiv.org/abs/2203.05461) [gr-qc].
- [41] E. R. Most, A. Motornenko, J. Steinheimer, V. Dexheimer, M. Hanauske, L. Rezzolla, and H. Stoecker, *Phys. Rev. D* **107**, 043034 (2023), [arXiv:2201.13150](https://arxiv.org/abs/2201.13150) [nucl-th].
- [42] Z. Zhu and L. Rezzolla, *Phys. Rev. D* **104**, 083004 (2021), [arXiv:2102.07721](https://arxiv.org/abs/2102.07721) [astro-ph.HE].
- [43] A. Prakash, I. Gupta, M. Breschi, R. Kashyap, D. Radice, S. Bernuzzi, D. Logoteta, and B. S. Sathyaprakash, *Phys. Rev. D* **109**, 103008 (2024), [arXiv:2310.06025](https://arxiv.org/abs/2310.06025) [gr-qc].
- [44] S. Blacker and A. Bauswein, arXiv e-prints, [arXiv:2406.14669](https://arxiv.org/abs/2406.14669) (2024), [arXiv:2406.14669](https://arxiv.org/abs/2406.14669) [astro-ph.HE].
- [45] M. Shibata, S. Karino, and Y. Eriguchi, *Mon. Not. Roy. Astron. Soc.* **343**, 619 (2003), [arXiv:astro-ph/0304298](https://arxiv.org/abs/astro-ph/0304298).
- [46] L. Baiotti, R. De Pietri, G. M. Manca, and L. Rezzolla, *Phys. Rev. D* **75**, 044023 (2007), [arXiv:astro-ph/0609473](https://arxiv.org/abs/astro-ph/0609473).
- [47] X. Xie, I. Hawke, A. Passamonti, and N. Andersson, *Phys. Rev. D* **102**, 044040 (2020), [arXiv:2005.13696](https://arxiv.org/abs/2005.13696) [astro-ph.HE].
- [48] K. Takami, L. Rezzolla, and L. Baiotti, *Phys. Rev. D* **91**, 064001 (2015), [arXiv:1412.3240](https://arxiv.org/abs/1412.3240) [gr-qc].
- [49] K. Takami, L. Rezzolla, and L. Baiotti, *Phys. Rev. Lett.* **113**, 091104 (2014), [arXiv:1403.5672](https://arxiv.org/abs/1403.5672) [gr-qc].
- [50] L. Rezzolla and K. Takami, *Phys. Rev. D* **93**, 124051 (2016), [arXiv:1604.00246](https://arxiv.org/abs/1604.00246) [gr-qc].
- [51] A. Prakash, D. Radice, D. Logoteta, A. Perego, V. Nedora, I. Bombaci, R. Kashyap, S. Bernuzzi, and A. Endrizzi, *Phys. Rev. D* **104**, 083029 (2021).
- [52] D. Reitze *et al.*, *Bull. Am. Astron. Soc.* **51**, 035 (2019), [arXiv:1907.04833](https://arxiv.org/abs/1907.04833) [astro-ph.IM].
- [53] K. Ackley *et al.*, *Publ. Astron. Soc. Austral.* **37**, e047 (2020), [arXiv:2007.03128](https://arxiv.org/abs/2007.03128) [astro-ph.HE].
- [54] S. Blacker, A. Bauswein, and S. Typel, *Phys. Rev. D* **108**, 063032 (2023), [arXiv:2304.01971](https://arxiv.org/abs/2304.01971) [astro-ph.HE].
- [55] S. Blacker, H. Kochankovski, A. Bauswein, A. Ramos, and L. Tolos, *Phys. Rev. D* **109**, 043015 (2024), [arXiv:2307.03710](https://arxiv.org/abs/2307.03710) [astro-ph.HE].
- [56] P. Bedaque and A. W. Steiner, *Phys. Rev. Lett.* **114**, 031103 (2015).
- [57] S. Vinciguerra, T. Salmi, A. L. Watts, D. Choudhury, T. E. Riley, P. S. Ray, S. Bogdanov, Y. Kini, S. Guillot, D. Chakrabarty, W. C. G. Ho, D. Huppenkothen, S. M. Morsink, Z. Wadiasingh, and M. T. Wolff, *Astrophys. J.* **961**, 62 (2024), [arXiv:2308.09469](https://arxiv.org/abs/2308.09469) [astro-ph.HE].
- [58] H. Togashi, K. Nakazato, Y. Takehara, S. Yamamuro, H. Suzuki, and M. Takano, *Nucl. Phys. A* **961**, 78 (2017), [arXiv:1702.05324](https://arxiv.org/abs/1702.05324) [nucl-th].
- [59] D. Lonardonì, I. Tews, S. Gandolfi, and J. Carlson, *Phys. Rev. Res.* **2**, 022033 (2020).
- [60] C. Drischler, J. W. Holt, and C. Wellenhofer, *Annual Review of Nuclear and Particle Science* **71**, 403 (2021), [arXiv:2101.01709](https://arxiv.org/abs/2101.01709) [nucl-th].
- [61] C. Drischler, S. Han, J. M. Lattimer, M. Prakash, S. Reddy, and T. Zhao, *Physical Review C* **103**, 10.1103/physrevc.103.045808 (2021).
- [62] F. Douchin and P. Haensel, *Astron. Astrophys.* **380**, 151 (2001), [arXiv:astro-ph/0111092](https://arxiv.org/abs/astro-ph/0111092).
- [63] A. Akmal, V. R. Pandharipande, and D. G. Ravenhall, *Phys. Rev. C* **58**, 1804 (1998).
- [64] J. M. Lattimer and F. D. Swesty, *Nucl. Phys. A* **535**, 331 (1991).
- [65] L. Rezzolla, L. Baiotti, B. Giacomazzo, D. Link, and J. A. Font, *Class. Quant. Grav.* **27**, 114105 (2010), [arXiv:1001.3074](https://arxiv.org/abs/1001.3074) [gr-qc].
- [66] Y.-Z. Fan, X.-F. Wu, and D.-M. Wei, *Phys. Rev. D* **88**, 067304 (2013), [arXiv:1302.3328](https://arxiv.org/abs/1302.3328) [astro-ph.HE].
- [67] N. Stergioulas, A. Bauswein, K. Zagkouris, and H.-T. Janka, *Mon. Not. R. Astron. Soc.* **418**, 427 (2011), [arXiv:1105.0368](https://arxiv.org/abs/1105.0368) [gr-qc].
- [68] C. Ecker, T. Gorda, A. Kurkela, and L. Rezzolla, Listening to the long ringdown: a novel way to pinpoint the equation of state in neutron-star cores (2024), [arXiv:2403.03246](https://arxiv.org/abs/2403.03246) [astro-ph.HE].
- [69] S. Bernuzzi, D. Radice, C. D. Ott, L. F. Roberts, P. Moesta, and F. Galeazzi, *Phys. Rev. D* **94**, 024023 (2016), [arXiv:1512.06397](https://arxiv.org/abs/1512.06397) [gr-qc].
- [70] S. V. Chaurasia, T. Dietrich, M. Ujevic, K. Hendriks, R. Dudi, F. M. Fabbri, W. Tichy, and B. Brügmann, *Phys. Rev. D* **102**, 024087 (2020), [arXiv:2003.11901](https://arxiv.org/abs/2003.11901) [gr-qc].

Neutron-quark stars: Discerning viable alternatives for the higher-density part of the equation of state of compact star (Supplemental Material)

Sudipta Hensh,^{1,2,*} Yong-Jia Huang,^{3,4,†} Toru Kojo,^{5,‡} Luca Baiotti,⁶
Kentaro Takami,^{7,4} Shigehiro Nagataki,^{2,4,8} and Hajime Sotani^{2,4}

¹*Department of Earth and Space Science, Graduate School of Science,
Osaka University, 1-1 Machikaneyama-cho, Toyonaka, Osaka 560-0043, Japan*

²*Astrophysical Big Bang Laboratory (ABBL), RIKEN Cluster for Pioneering Research, 2-1 Hirosawa, Wako, Saitama 351-0198, Japan*

³*Key Laboratory of Dark Matter and Space Astronomy,*

Purple Mountain Observatory, Chinese Academy of Science, Nanjing, 210008, China

⁴*RIKEN Interdisciplinary Theoretical and Mathematical Sciences Program (iTHEMS), RIKEN, Wako 351-0198, Japan*

⁵*Department of Physics, Tohoku University, Sendai, 980-8578, Japan*

⁶*International College and Graduate School of Science, Osaka University,
1-2 Machikaneyama-cho, Toyonaka, Osaka 560-0043, Japan*

⁷*Kobe City College of Technology, 651-2194 Kobe, Japan*

⁸*Astrophysical Big Bang Group (ABBG), Okinawa Institute of Science and Technology (OIST),
1919-1 Tancha, Onna-son, Kunigami-gun, Okinawa 904-0495, Japan*

(Dated: August 5, 2024)

I. EQUATIONS OF STATE

A. Nuclear equations of state

We consider a nuclear EOS with leptons, the Togashi EOS [1], and the ChEFTex EOS based on Refs. [2–4]. The Togashi EOS is based on variational calculations with microscopic two- and three-body nuclear forces constrained by scattering experiments and spectroscopy of light nuclei. The EOS tables are given from the crust to very high density domains with consistent use of nuclear forces.

The ChEFTex EOS is based on the ChEFT calculations for nuclear liquid from baryon number density $n_B = 0.5n_0$ to $1.5n_0$ with supplemental treatments for $n_B < 0.5n_0$ and $n_B > 1.5n_0$. For $n_B < 0.5n_0$, the nuclear liquid picture is not trustable and we use a crust EOS. For $n_B > 1.5n_0$, ChEFT is not valid so EOS tables for $n_B > 1.5n_0$ are based on extrapolation: we use a parametrization up to cubic polynomials, $\varepsilon = \sum_{n=0}^3 c_n (n_B/n_0)^n$, with the coefficients c_n 's determined by the fit to quantities provided in ChEFT in the range $[0.5, 1.5]n_0$.

Roughly speaking, the power of density, N , characterizes N -body short-range repulsion. At very large density, the energy density scales as $\varepsilon \sim c_3 (n_B/n_0)^3$ and the corresponding pressure is $P = n_B^2 \partial(\varepsilon/n_B)/\partial n_B \sim 2\varepsilon$. Thus the sound speed asymptotically approaches $c_s^2 \sim 2c^2$. The dominance of three-body forces and the associated growth of c_s^2 are helpful to satisfy the $2M_\odot$ constraints, but this eventually violates the causality bound. In the ChEFTex EOS the causality violation occurs at $\approx 6.4n_0$, and, for the Togashi EOS, at $\sim 5.5n_0$. For both EOSs, such densities are not reached in our simulations. Since nuclear EOSs predict a gentle stiffening with increasing density, the radius of higher-mass ($2.1M_\odot$) stars is slightly smaller than that of lower-mass ($1.4M_\odot$) stars: $R_{1.4} - R_{2.1} \approx 1$ km.

B. Hybrid equations of state with a first-order phase transition

In our hybrid EOS with a 1PT, 1PT-NQS, we use the ChEFTex EOS up to $1.8n_0$ and an EOS with constant sound speed at densities past the transition. In order to avoid significant violations of the observational constraints while keeping the 1PT nature visible (a 1PT at densities near the maximum allowed for NSs would also be consistent with current observations, but would lead to prompt collapse after the merger and, thus, to no post-merger GW radiation), we choose $c_s^2 = 2/3 c^2$ in the quark matter part while demanding the 1PT to occur at $\approx 1.8n_0$ and end at $\approx 2.75n_0$. In this setup, the stars in our simulations already contain quark matter in their core before the merger and the stellar radius at $\sim 1.4M_\odot$ is smaller than the one for the ChEFTex EOS. This is a novel choice for initial conditions for numerical-relativity simulations; to the best of our knowledge, in all previous general-relativistic numerical work on BNSs with 1PT EOSs, the transition occurred after the merger. Since it is challenging to produce, with codes based on spectral methods, initial data (for simulations) that contain discontinuities, we resorted to smoothing out the discontinuities in c_s^2 (see. Fig. 1 of the main text). To avoid any thermodynamic inconsistency, such smoothing was done at the level of $P(\mu_B)$, and we derived all the other thermodynamic quantities from the differentiation of $P(\mu_B)$ with respect to μ_B .

C. Quark-hadron-crossover equations of state

QHC EOSs [5] are produced by using different combinations of nuclear and quark-matter EOSs in the lower- and upper-density ranges. We use a nuclear EOS for $n_B \leq 1.5n_0$ and a quark-matter EOS for $n_B \geq 3.5n_0$; in between, the

TABLE I. Characteristics of the simulated BNS merger systems: The table presents various properties of the BNS merger systems studied in this work. The listed quantities, ordered from left to right, are the gravitational mass (M) of one isolated star, baryon mass (M_b) of one star, radius (R) of one isolated non-rotating star, Arnowitt-Deser-Misner (ADM) mass of the BNS system (M_{ADM}) at the initial time, total angular momentum (J) at the initial time, orbital frequency (f_{orb}) at the initial time, dimensionless tidal deformability Λ , contact frequency ($f_{\text{cont}} = C^3/2\pi M$, where C is compactness, namely the ratio of gravitational mass to the radius), post-merger peak frequency (f_2) with its 68% confidence interval, and the mean frequency of the f_2 peak ($f_{2,\text{mean}}$). The units corresponding to these quantities are specified in the square brackets adjacent to each.

Model	$M[M_\odot]$	$M_b[M_\odot]$	$R[\text{km}]$	$M_{\text{ADM}}[M_\odot]$	$J[M_\odot^2]$	$f_{\text{orb}}[\text{Hz}]$	Λ	$f_{\text{cont}}[\text{Hz}]$	$f_2[\text{Hz}]$	$f_{2,\text{mean}}[\text{Hz}]$
QHC21Ch-soft-M1.25	1.25	1.36	12.32	2.48	6.4	273.03	854	1499.04	2443_{-4}^{+4}	2795
QHC21Ch-soft-M1.375	1.375	1.51	12.36	2.72	7.5	283.47	502	1564.59	2617_{-2}^{+1}	2995
QHC21Ch-soft-M1.375 ($\Delta x = 185m$)	1.375	1.51	12.36	2.72	7.5	283.47	502	1564.59	2672_{-5}^{+6}	2940
QHC21Ch-soft-M1.375 ($\Delta x = 288m$)	1.375	1.51	12.36	2.72	7.5	283.47	502	1564.59	2633_{-9}^{+10}	2982
QHC21Ch-soft-M1.48	1.48	1.64	12.39	2.92	8.48	291.69	329	1617.33	2938_{-4}^{+4}	3138
QHC21Ch-stiff-M1.25	1.25	1.36	12.29	2.48	6.4	273.04	841	1504.54	2512_{-23}^{+24}	2840
QHC21Ch-stiff-M1.375	1.375	1.51	12.33	2.72	7.5	283.44	495	1570.3	2676_{-23}^{+20}	3025
QHC21Ch-stiff-M1.48	1.48	1.64	12.37	2.92	8.48	291.77	326	1623.23	2688_{-6}^{+6}	3114
QHC21T-soft-M1.25	1.25	1.37	11.77	2.48	6.4	273.02	693	1605.34	2648_{-7}^{+7}	2964
QHC21T-soft-M1.375	1.375	1.52	11.84	2.72	7.49	283.47	411	1668.78	2824_{-6}^{+6}	3171
QHC21T-soft-M1.43	1.43	1.59	11.87	2.82	8.00	287.79	329	1695.38	2896_{-4}^{+4}	3211
QHC21T-stiff-M1.25	1.25	1.37	11.68	2.48	6.39	272.97	657	1623.93	2642_{-19}^{+26}	2980
QHC21T-stiff-M1.375	1.375	1.52	11.75	2.72	7.5	283.52	389	1687.99	2719_{-2}^{+1}	3126
QHC21T-stiff-M1.43 ($\Delta x = 185m$)	1.43	1.59	11.78	2.82	8.00	287.73	313	1714.85	2750_{-10}^{+11}	3254
Togashi-M1.125	1.25	1.37	11.57	2.47	6.39	273.00	587	1647.29	2802_{-11}^{+11}	3147
Togashi-M1.375	1.375	1.52	11.58	2.72	7.49	283.39	329	1898.25	2979_{-6}^{+7}	3226
ChEFTex-M1.25	1.25	1.36	12.21	2.48	6.39	272.93	784	1519.35	2645_{-10}^{+11}	2886
ChEFTex-M1.375	1.375	1.51	12.17	2.72	7.49	283.45	437	1526.84	2946_{-4}^{+4}	3170
1PT-NQS-M1.25	1.25	1.36	11.50	2.48	6.40	273.11	489	1662.20	2904_{-5}^{+5}	3259
1PT-NQS-M1.375	1.375	1.52	11.47	2.72	7.49	283.10	277	1750.18	3075_{-7}^{+7}	3483
1PT-NQS-M1.375 ($\Delta x = 185m$)	1.375	1.52	11.47	2.72	7.49	283.10	277	1750.18	3075_{-9}^{+9}	3497
1PT-NQS-M1.375 ($\Delta x = 288m$)	1.375	1.52	11.47	2.72	7.49	283.10	277	1750.18	3045_{-7}^{+7}	3549

EOS is constructed by interpolating the nuclear and quark-matter EOSs. The interpolating functions are polynomials $P(\mu_B) = \sum_{n=0}^5 c_n \mu_B^n$ with the coefficients that are demanded to match with the nuclear and quark-matter EOSs up to second-order derivatives. The quark EOS contains two variable parameters for the effective repulsion and the attractive correlations in diquark channels [5].

The reader is referred to the main text to see the abbreviations we use for the different variants of QHC EOSs and 1PT EOS. The QHC EOSs used in this work are publicly available through the ComPOSE database <https://compose.obspm.fr/>.

II. NUMERICAL SETUP

In this section, we discuss the numerical setup that was used to perform BNS merger simulations.

We produced initial data for quasi-equilibrium irrotational equal-mass BNS configurations with an initial separation of 45 km, resulting in approximately 8 to 12 orbits before the merger, depending on the model. This was accomplished through the multi-domain pseudo-spectral open-source code Lorene [6].

We use the open-source high-resolution shock-capturing fully general-relativistic hydrodynamic code WhiskyTHC [7, 8], which is based on the Einstein Toolkit [9] framework. Specifically, our computational approach for hydrodynamics involves the utilization of a finite-volume scheme featuring advanced 5th-order monotonicity-preserving reconstruction techniques [10]. The Riemann problems within the scheme are handled with the Harten-Lax-van Leer-Einfeldt (HLLC) Riemann solver [11]. The evolution of spacetime is computed utilizing the Z4c formulation [12, 13] through the CTGamma code, which implements “1 + log” slicing for the lapse function and “Gamma-driver” shift conditions [14]. The time integration of the hydrodynamics and Einstein equations is carried out with the method of lines, employing a third-order strong-stability-preserving Runge-Kutta scheme [15], chosen for its efficacy in maintaining stability. We set the Courant-Friedrichs-Lewy (CFL) factor to 0.075. This stringent choice is crucial when implementing flux reconstruction in local-characteristic variables, a technique integral to our adopted monotonicity-preserving scheme [10]. For adaptive-mesh refinement (AMR), we use the Carpet code [16], with seven refinement levels. Our outer boundary is set at 1477 km.

We examined the dependence of f_2 on numerical resolution using the QHC21Ch-soft and 1PT-NQS models with mass $2.75 M_\odot$ at three different resolutions: Low (finest grid spacing ($\Delta x \approx 369$ m), Medium ($\Delta x \approx 231$ m), and High ($\Delta x \approx 185$ m). As shown in table I, the post-merger frequencies, like other post-merger quantities, do not converge with resolution (this is usually observed in current simulations with other codes too). Conservatively, we assume the differences between the f_2 at different resolutions to be our error on them. This is about 50 Hz and is larger than the error due to the fitting procedure (*cf.* Table I).

III. MATTER EVOLUTION

To give an overview of the simulation results, in Figs. S1 and S2 we show isocontours of the number density at selected times, before, during, and after the merger. The black lines are the onset density for the phase transition or the crossover, and the cyan lines are the densities beyond which all matter has turned to quark matter.

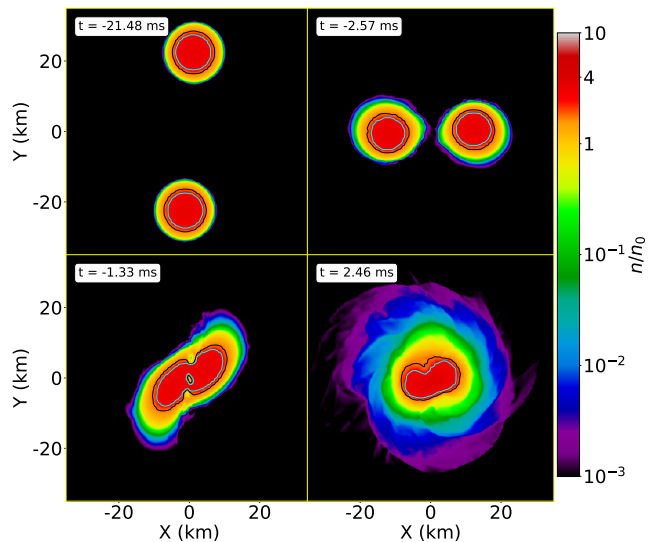


FIG. S1. Isodensity contours on the (x,y) (equatorial) plane for the BNS with our 1PT-NQS EOS and mass $2.5M_\odot$. The black lines show the number density of the onset of the 1PT. The cyan lines show the number density above which only quark matter is present. The colorbar refers to number density in units of nuclear density. The values shown in the time stamps are such that the time of the merger is $t = 0$.

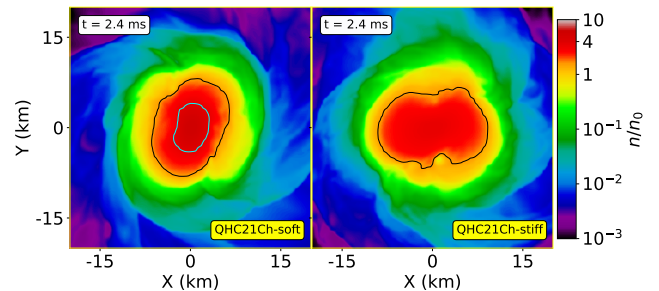


FIG. S2. As in Fig. S1 but for the QHC21Ch models with the highest mass, $2.96M_\odot$, at time $t = 2.4$ ms after the merger. The black contour lines show the number density of the onset of the QHC. The cyan contour line shows the number density above which only quark matter is present.

The upper-left panel of Fig. S1 shows that quark matter is already present in the inspiralling stars for our 1PT-NQS EOS. In the upper-right panel, referring to just before the merger defined - as usual - by the maximum of the amplitude of the GW signal, we see that the quark-matter cores are deformed, but to a lesser degree with respect to hadronic matter and the mixed phase. At the time of the lower-left panel, also the quark-matter cores have merged, even if at the center matter is not purely quarks. The lower-right panel shows the deformed merged object.

Fig. S2 refers to the QHC21 models for the highest-mass case, about 2.4 ms after the merger. The black contour represents the low-density boundary of the quark-hadron

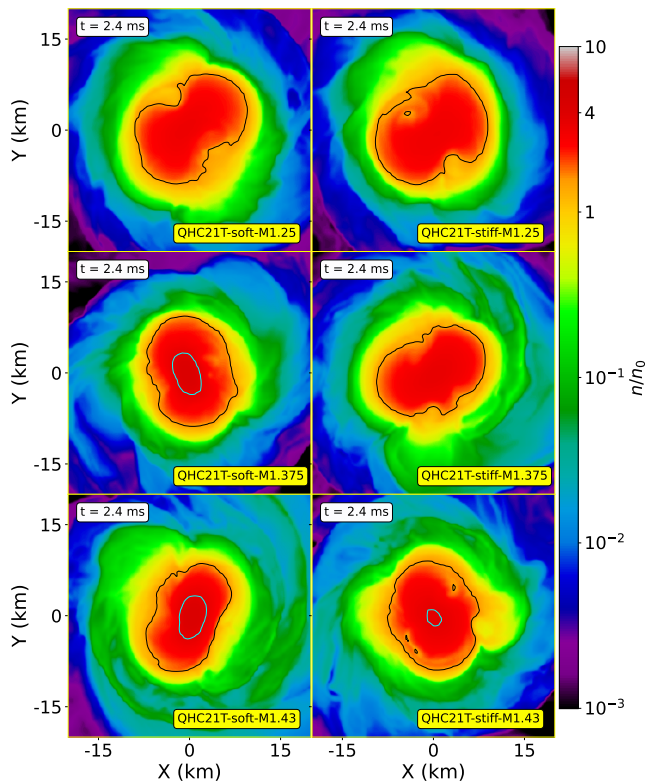


FIG. S3. Isodensity contours on the (x,y) (equatorial) plane at a time $t = 2.4$ ms after the merger for the QHC21T models with different masses. The black contour lines show the density of the onset of the QHC. The cyan contour lines show the density above which only quark matter is present. The colorbar refers to number density in units of nuclear density.

crossover, while inside the cyan contour pure quark matter is present. As seen in Fig. 1 of the main text, at the density of the cores of these objects QHC21Ch-soft is softer than QHC21Ch-stiff and, indeed, the left panel, for QHC21Ch-soft, shows that higher densities are reached, including a region of pure quark matter, still absent in the QHC21Ch-stiff case.

In Fig. S3, we show 2D snapshots of the number density for the QHC21T models.

The evolution of the maximum of the number density n_{\max} for the QHC21 EOSs is shown in Fig. S4 and that for the 1PT-NQS EOS in Fig. S5. Core densities in both types of models are over the threshold for the presence of quark degrees of freedom, also before the merger.

IV. ADDITIONAL ANALYSES

In table I, we report some properties of the BNS merger systems simulated in this work including the dimensionless tidal deformability, $\Lambda = 32k_2(R/M)^5$, where M is the gravitational mass, R is the radius of the isolated star, and k_2 is the tidal love number [17–19].

In Fig. S7, we show the values of the f_2 frequency for different binary masses and EOSs. The error bands in the figure refer to the fitting error (see our previous work [20] for details). However, note again that the conservative estimate for the total uncertainty on our results for f_2 , including considerations on finite resolution, is about 50 Hz.

In order to interpret the relations between the f_2 frequencies for different EOSs, it is useful to consider how stiffer or softer they are in the relevant density ranges. This can be understood from examining the sound speed c_s^2 as a function of density, in Fig. 1 of the main text. At a given density, stiffer EOSs have a higher value of c_s^2 . Starting our comments from the lower frequencies, we see that the differences between the f_2 for QHC21Ch-soft and QHC21Ch-stiff for the lower-mass cases are about as large as our estimate of the total uncertainty and therefore should be considered indistinguishable in the current work. For the same EOSs but for the highest-mass case, the difference in f_2 is relevant, the one for QHC21Ch-soft being higher, as expected from the fact that QHC21Ch-soft is softer than QHC21Ch-stiff in the density range of the core of the merged object (*cf.* Fig. S4 and Fig. 1 in the main text).

However, more interesting is to notice that f_2 for both QHC21Ch models is significantly lower than that of the baseline EOS, the ChEFTex EOS, which has no transitions to quark matter (note that we performed also simulations for the ChEFTex EOS with higher masses than shown in the figure, but they resulted in a prompt collapse to a black hole).

This result applies to the QHC21T models as well, namely, their f_2 frequencies are always significantly lower than those of their baseline EOS, the Togashi EOS (for the Togashi EOS too, we performed simulations with higher masses than shown in the figure, but they resulted in a prompt collapse to a black hole). The general result that f_2 for the hadronic baseline EOSs is significantly higher than that of their corresponding QHC models confirms and extends our previous findings [20] and is due to the fact that, in the density ranges reached after the merger, our hadronic baseline EOSs are much stiffer than their corresponding QHC models (*cf.* Fig. S4 and Fig. 1 in the main text).

These findings on the relations of the f_2 of different QHC models is consistent with what seen in Fig. S4, namely, that the density reached in the core of stars with the QHC21 and QHC21T EOSs are smaller than those reached in the respective baseline EOSs, and with what seen in the *upper panels* of Fig. S8, namely, that the loss of angular momentum observed in the QHC models is lower than that of their baseline hadronic EOSs.

We also note the consistency between the f_2 values for the QHC21T models and the extent of their quark cores. The f_2 for the low-mass case of the QHC21T models are similar, as similar are the sizes of the quark-hadron mixed phase cores (black contour in the top panels of Fig. S3). On

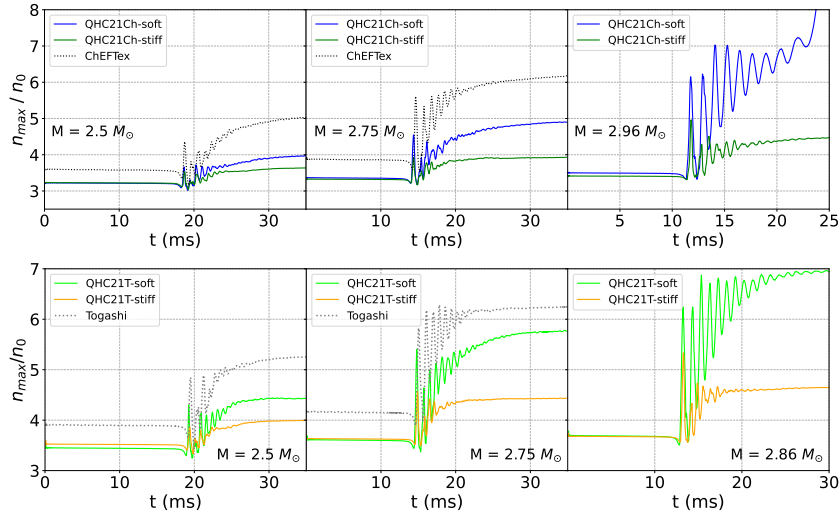


FIG. S4. Evolution of the maximum number density in units of nuclear saturation density for the QHC21 and QHC21T EOSs and their baseline EOSs, for different binary masses.

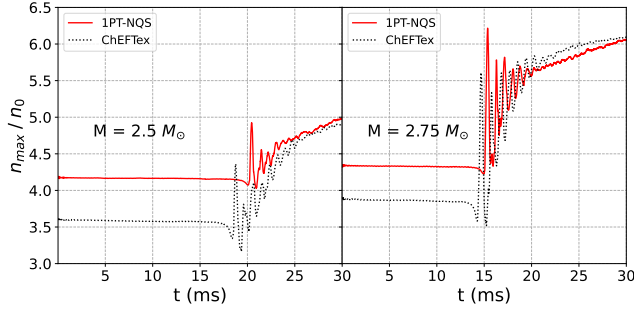


FIG. S5. Evolution of the maximum number density in units of nuclear saturation density for the 1PT-NQS EOS and its baseline EOS, for different binary masses.

the other hand, for intermediate- and high-mass scenarios, f_2 is higher for the QHC21T-soft EOS. This is consistent with QHC21T-soft having a larger quark-matter core, as seen in the middle and bottom panels of Fig. S3 (QHC21T-stiff-M1.375 does not have a quark-matter core at the time of the snapshot).

Finally, note that the values of f_2 for the 1PT-NQS models are much higher than those of any other EOS. This is expected because the stars with the 1PT-NQS EOS have significantly smaller radii and thus merge later (*cf.* Fig. S5), leaving a faster rotating merged object, with a higher f_2 frequency.

Fig. S8 shows the time evolution of the angular momentum (upper panels) and energy (lower panels) emitted in GWs. It is interesting to note that for the 1PT-NQS EOSs, the angular momentum and energy carried away by GWs after the merger are larger than in any other model (with the exception of the unrelated Togashi EOS for the intermediate-mass case). This may be due to different de-

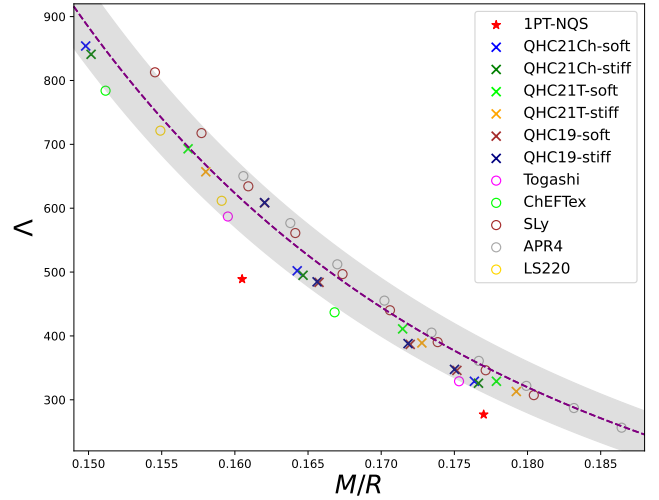


FIG. S6. Scatter plot of dimensionless tidal deformability and compactness for various EOSs. Red stars are for the 1PT-NQS EOS, crosses are for the QHC models, including QHC19, from [20], while the open circles are for the hadronic EOSs considered in this work and SLy, APR4, LS220, taken from [21]. The dashed curve is the best fit considering the fitting relation, $\Lambda = \gamma + \frac{\delta}{(M/R)^5}$, where the parameters from the fit are $\gamma = -59.23 \pm 24.29$ and $\delta = 0.071 \pm 0.003$.

formations in the merged object, which may include odd modes. We will leave this analysis to future work.

Here, we add further comments to what we say in the main text about the relation between the energy and the angular momentum radiated in GWs after the merger. For different masses, in Fig. S9 we compare graphs of the relation using non-normalized post-merger-only quantities or normalized quantities. In the low-mass case with nor-

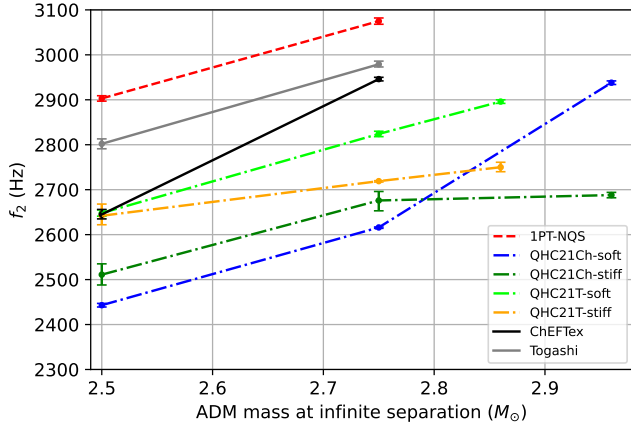


FIG. S7. The f_2 frequency as a function of binary mass (the ADM mass of the binary at infinite separation) for various EOS models. Error bars are estimated in the fitting procedure.

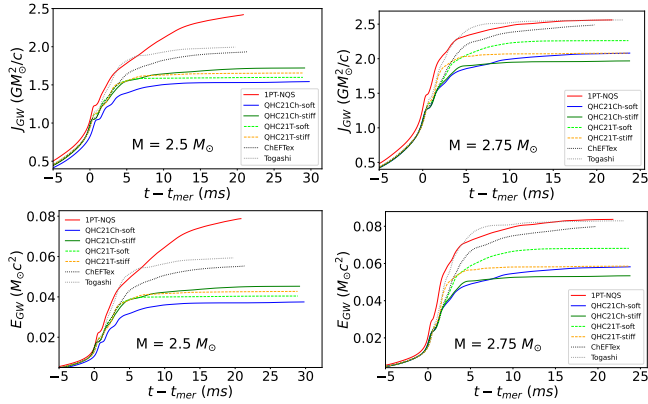


FIG. S8. Radiated angular momentum (*upper panels*) and energy (*lower panels*), as a function of time. $t = t_{\text{mer}}$ is the time of merger.

malized quantities, the 1PT-NQS EOS and some of the QHC models can be somewhat distinguished. However, for the intermediate-mass case, the deviations are much smaller. The reason for this could be that we stopped our intermediate-mass simulations earlier. Longer post-merger simulations may be required to reproduce better the results of previous studies [22]. In any case, we can see that in the relation that considers non-normalized post-merger-only quantities the curve for 1PT-NQS deviates even more from those of the other models, especially in the intermediate-mass case. Also the curves of the other models are further apart.

Finally, we were inspired by the results discussed in [23] to study the lifetime of the merged object, namely, the time between merger and collapse to black hole, with our setup and EOSs. In [23], a *weak* dependence of the lifetime on Γ_{th} and grid resolution was reported. That being a qualitative study on this point, we were motivated to test the assertions quantitatively. As discussed earlier, the effective

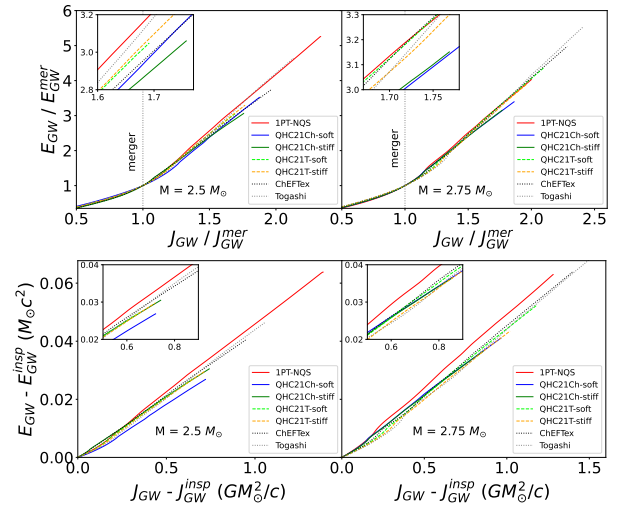


FIG. S9. Radiated energy as a function of radiated angular momentum. The top panels show the relation between quantities normalized to their values at the time of merger. The bottom panels show quantities calculated excluding the inspiral contribution.

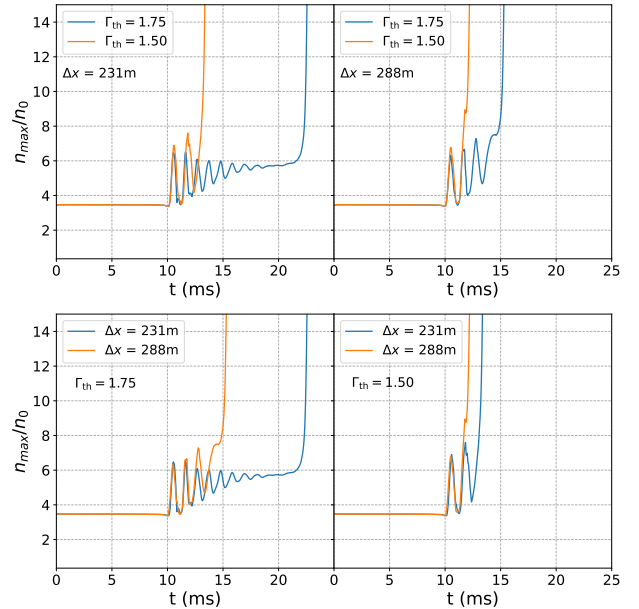


FIG. S10. Evolution of the maximum of the number density (n_{max}) in units of nuclear saturation density for the QHC21Ch-stiff EOS model with mass $3.1 M_{\odot}$ and different combinations of Γ_{th} and grid spacing of the finest refinement level, Δx .

temperature treatment performed by adding a *hot* component to the EOS through an ideal-fluid EOS with index Γ_{th} increases pressure support in the merged object. Therefore, a change in the value of the Γ_{th} index directly impacts the lifetime. Furthermore, it is interesting to quantitatively investigate the influence of grid resolution.

To have a similar setup to that of [23], we investigated

the cases of $\Gamma_{\text{th}} = 1.5$ and $\Gamma_{\text{th}} = 1.75$. We performed simulations of a binary system of mass $3.1M_{\odot}$ with the QHC21Ch-stiff EOS, and at two resolutions: finest grid spacing of 231 m and 288 m. This mass was selected to have a timescale for the lifetime comparable to that of the aforementioned study. We let the evolution continue until an apparent horizon [24, 25] was found. The evolution of the maximum number density for different configurations is shown in Fig. S10. From the top panels, one can compare the lifetime for different values of Γ_{th} and for different grid resolutions. The top-left panel points out a notable 41% difference in the lifetime between the cases of different Γ_{th} for the higher resolution, whereas this difference decreases to approximately 20% for the lower resolution (top-right panel). In the bottom panels, the lifetime for a choice of Γ_{th} with different finest-grid spacings is presented. The change in lifetime is about 32% for different resolutions for $\Gamma_{\text{th}} = 1.75$ (bottom-left panel), while it is 9% for $\Gamma_{\text{th}} = 1.5$ (bottom-right panel). In conclusion, we can say that there is a non-negligible dependence of the lifetime on Γ_{th} and on grid resolution.

* hensh@astro-osaka.jp, sudiptahensh2009@gmail.com

† huangyj@pmo.ac.cn

‡ toru.kojo.b1@tohoku.ac.jp

- [1] H. Togashi, K. Nakazato, Y. Takehara, S. Yamamuro, H. Suzuki, and M. Takano, *Nucl. Phys. A* **961**, 78 (2017), [arXiv:1702.05324](https://arxiv.org/abs/1702.05324) [nucl-th].
- [2] D. Lonardoni, I. Tews, S. Gandolfi, and J. Carlson, *Phys. Rev. Res.* **2**, 022033 (2020).
- [3] C. Drischler, J. W. Holt, and C. Wellenhofer, *Annual Review of Nuclear and Particle Science* **71**, 403 (2021), [arXiv:2101.01709](https://arxiv.org/abs/2101.01709) [nucl-th].
- [4] C. Drischler, S. Han, J. M. Lattimer, M. Prakash, S. Reddy, and T. Zhao, *Physical Review C* **103**, 10.1103/physrevc.103.045808 (2021).
- [5] T. Kojo, G. Baym, and T. Hatsuda, *Astrophys. J.* **934**, 46 (2022), [arXiv:2111.11919](https://arxiv.org/abs/2111.11919) [astro-ph.HE].
- [6] E. Gourgoulhon, P. Grandclément, K. Taniguchi, J.-A. Marck, and S. Bonazzola, *Phys. Rev. D* **63**, 064029 (2001).
- [7] D. Radice, L. Rezzolla, and F. Galeazzi, *Monthly Notices of the Royal Astronomical Society: Letters* **437**, L46 (2013).
- [8] D. Radice, L. Rezzolla, and F. Galeazzi, *Class. Quant. Grav.* **31**, 075012 (2014), [arXiv:1312.5004](https://arxiv.org/abs/1312.5004) [gr-qc].
- [9] L. Werneck, S. Cupp, T. Assumpção, and S. R. B. et al., *The einstein toolkit* (2023), to find out more, visit <http://einstein toolkit.org>.
- [10] A. Suresh and H. T. Huynh, *Journal of Computational Physics* **136**, 83 (1997).
- [11] A. Harten, P. D. Lax, and B. v. Leer, *SIAM review* **25**, 35 (1983).
- [12] C. Bona, T. Ledvinka, C. Palenzuela, and M. Zacek, *Phys. Rev. D* **67**, 104005 (2003), [arXiv:gr-qc/0302083](https://arxiv.org/abs/gr-qc/0302083).
- [13] C. Bona and C. Palenzuela, *Phys. Rev. D* **69**, 104003 (2004), [arXiv:gr-qc/0401019](https://arxiv.org/abs/gr-qc/0401019).
- [14] M. Alcubierre, B. Bruegmann, P. Diener, M. Koppitz, D. Pollney, E. Seidel, and R. Takahashi, *Phys. Rev. D* **67**, 084023 (2003), [arXiv:gr-qc/0206072](https://arxiv.org/abs/gr-qc/0206072).
- [15] S. Gottlieb, D. I. Ketcheson, and C.-W. Shu, *Journal of Scientific Computing* **38**, 251 (2009).
- [16] E. Schnetter, S. H. Hawley, and I. Hawke, *Classical and Quantum Gravity* **21**, 1465 (2004).
- [17] T. Hinderer, *Astrophys. J.* **677**, 1216 (2008), [Erratum: *Astrophys. J.* 697, 964 (2009)], [arXiv:0711.2420](https://arxiv.org/abs/0711.2420) [astro-ph].
- [18] T. Hinderer, *The Astrophysical Journal* **697**, 964 (2009).
- [19] L. Lindblom and N. M. Indik, *Phys. Rev. D* **89**, 064003 (2014), [Erratum: *Phys. Rev. D* 93, 129903 (2016)], [arXiv:1310.0803](https://arxiv.org/abs/1310.0803) [astro-ph.HE].
- [20] Y.-J. Huang, L. Baiotti, T. Kojo, K. Takami, H. Sotani, H. Togashi, T. Hatsuda, S. Nagataki, and Y.-Z. Fan, *Phys. Rev. Lett.* **129**, 181101 (2022).
- [21] L. Rezzolla and K. Takami, *Phys. Rev. D* **93**, 124051 (2016), [arXiv:1604.00246](https://arxiv.org/abs/1604.00246) [gr-qc].
- [22] C. Ecker, T. Gorda, A. Kurkela, and L. Rezzolla, Listening to the long ringdown: a novel way to pinpoint the equation of state in neutron-star cores (2024), [arXiv:2403.03246](https://arxiv.org/abs/2403.03246) [astro-ph.HE].
- [23] Y. Fujimoto, K. Fukushima, K. Hotokezaka, and K. Kyutoku, *Phys. Rev. Lett.* **130**, 091404 (2023), [arXiv:2205.03882](https://arxiv.org/abs/2205.03882) [astro-ph.HE].
- [24] J. Thornburg, *Living Reviews in Relativity* **10**, 3 (2007).
- [25] J. Thornburg, *Class. Quantum Grav.* **21**, 3665 (2004), [gr-qc/0404059](https://arxiv.org/abs/gr-qc/0404059).